RESEARCH ARTICLE OPEN ACCESS

Adaptive Threshold-Enhanced Deep Segmentation of Acute Intracranial Hemorrhage and Its Subtypes in Brain CT Images

R. Suganthi¹, Pratibha C. Kaladeep Yalagi², Rini Chowdhury ³, Prashant Kumar³, D. Sharmila⁴, Kunchanapalli Rama Krishna K⁵

- ¹ Department of Electronics and Communication Engineering, Panimalar Engineering College, Bangalore trunk road, Varadharajapuram, Poonamallee, Chennai, 600123, Tamil Nadu, India.
- ² Department of Computer Science and Engineering, Walchand Institute of Technology, Solapur, Maharashtra, India
- ³ Department of Information Technology Project Circle, Bharat Sanchar Nigam Limited, Saltlake Telephone Exchange, Block DE, Lalkuthi, West Bengal, Kolkata 700064, India.
- ⁴ Department of Electronics and Communication Engineering, Sri Krishna College of Engineering and Technology, BK Pudur, Kuniyamuthur, Tamil Nadu 641008, India
- ⁵ Department of Computer Science & Engineering, Koneru Lakshmaiah Education Foundation, Vaddeswaram, Guntur District -522302, Andhra Pradesh, India.

Corresponding author: Dr.R.Suganthi (e-mail : sugimanicks@gmail.com), Author(s) Email: Pratibha C. Kaladeep Yalagi (e-mail: pratibhayalagi@gmail.com), Rini Chowdhury (e-mail: chowdhury.rini@gmail.com), Prashant Kumar (e-mail: k21prashant@gmail.com), Dr.D.Sharmila (e-mail: Email: sharmilad@skcet.ac.in), Dr.Kunchanapalli Rama Krishna (e-mail: tenalirama@kluniversity.in),

ABSTRACT Accurate segmentation of acute intracranial haemorrhage (ICH) in brain computed tomography (CT) scans is crucial for timely diagnosis and effective treatment planning. While the RSNA Intracranial Hemorrhage Detection dataset provides a substantial amount of labeled CT data, most prior research has focused on slice-level classification rather than precise pixel-level segmentation. To address this limitation, a novel segmentation pipeline is proposed that combines a 2.5D U-Net architecture with a dynamic adaptive thresholding technique for enhanced delineation of hemorrhagic lesions and their subtypes. The 2.5D U-Net model leverages spatial continuity across adjacent slices to generate initial lesion probability maps, which are subsequently refined using an adaptive thresholding method that adjusts based on local pixel intensity histograms and edge gradients. Unlike fixed global thresholding approaches such as Otsu's method, the proposed technique dynamically varies thresholds, enabling more accurate differentiation between hemorrhagic tissue and surrounding brain structures, especially in challenging cases with diffuse or overlapping boundaries. The model was evaluated on carefully selected subsets of the RSNA dataset, achieving a mean Dice similarity coefficient of 0.82 across all ICH subtypes. Compared to standard U-Net and DeepLabV3+ architectures, the hybrid approach demonstrated superior accuracy, boundary precision, and fewer false positives. Visual analysis confirmed more precise lesion delineation and better correspondence with manual annotations, particularly in low-contrast or complex anatomical regions. This integrated approach proves effective for robust segmentation in clinical environments. It holds promise for deployment in computer-aided diagnosis systems, providing radiologists and neurosurgeons with a reliable tool for comprehensive ICH assessment and enhanced decision-making during emergency care.

Keywords Intracranial Hemorrhage; Brain Segmentation; RSNA Dataset; Adaptive Thresholding; Deep Learning; U-Net; Hemorrhage Subtypes.

I. Introduction

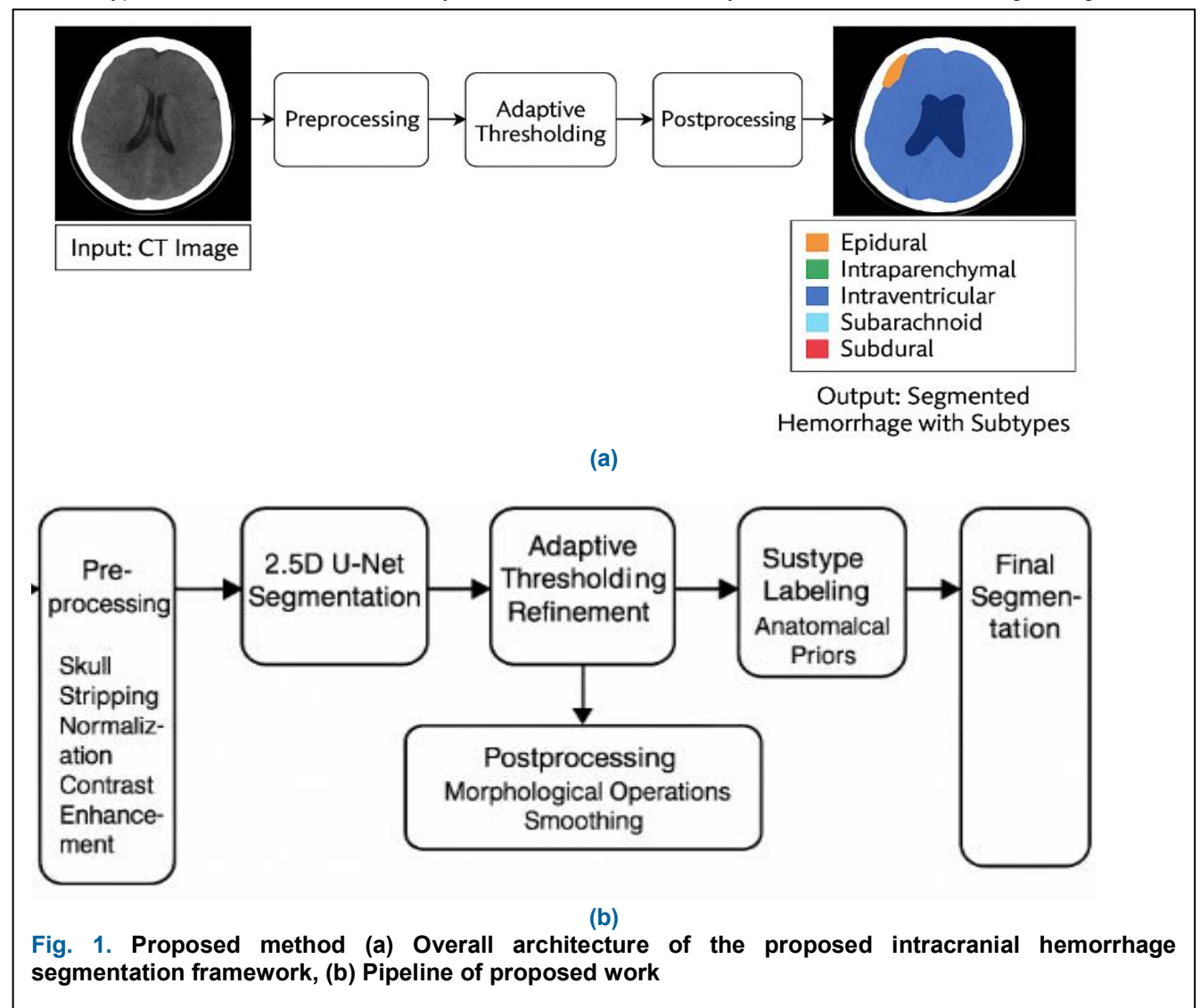
Intracranial hemorrhage (ICH) is bleeding within the cranial vault, which may be secondary to trauma, hypertension, aneurysm rupture, or any other underlying

illness [1]. It is a neurological emergency with serious and immediate implications that necessitate prompt diagnosis and treatment. Non-contrast computed tomography (CT) scans are the imaging technique most

frequently employed for ICH detection because of their quick scan time and acute blood sensitivity [2]. Though precise interpretation of CT scans requires significant clinical skill and can be hindered by inter-observer variation, notably in emergency or high-volume clinics. As the global incidence of stroke and neurotrauma continues to increase, there is an urgent need for the development of computer-aided diagnostic systems to support clinical practice and improve patient outcomes [3].

Although CT scans provide essential information for diagnosing intracranial hemorrhages (ICH), manually processing large imaging datasets remains inefficient, especially in urgent clinical settings where time is critical [4]. Automated and accurate segmentation of ICH is therefore vital to assist clinicians in precisely localizing hemorrhages, measuring their volume, and identifying their subtype distribution, which directly influences

treatment decisions and outcomes [5]. Differentiating between hemorrhage subtypes, such as subdural, epidural, intraparenchymal, subarachnoid, intraventricular, is particularly important because each subtype requires distinct management strategies. Despite progress in image classification using deep learning, there are relatively few models capable of delivering high-resolution, subtype-specific segmentation that accurately delineates hemorrhage boundaries at the pixel level [6]. This research aims to bridge this gap by introducing a novel technique that achieves precise demarcation of ICH regions and subtype classification on a pixel-wise basis, thereby enhancing the reliability and speed of diagnosis and supporting optimal treatment planning [7]. Deep learning models, especially convolutional neural networks (CNNs) such as U-Net and DeepLabV3+, have been extensively used in medical image segmentation



Journal of Electronics, Electromedical Engineering, and Medical Informatics

Homepage: <u>jeeemi.org</u>; Vol. 7, No. 4, October 2025, pp: 1289-1302 e-ISSN: <u>2656-8632</u>

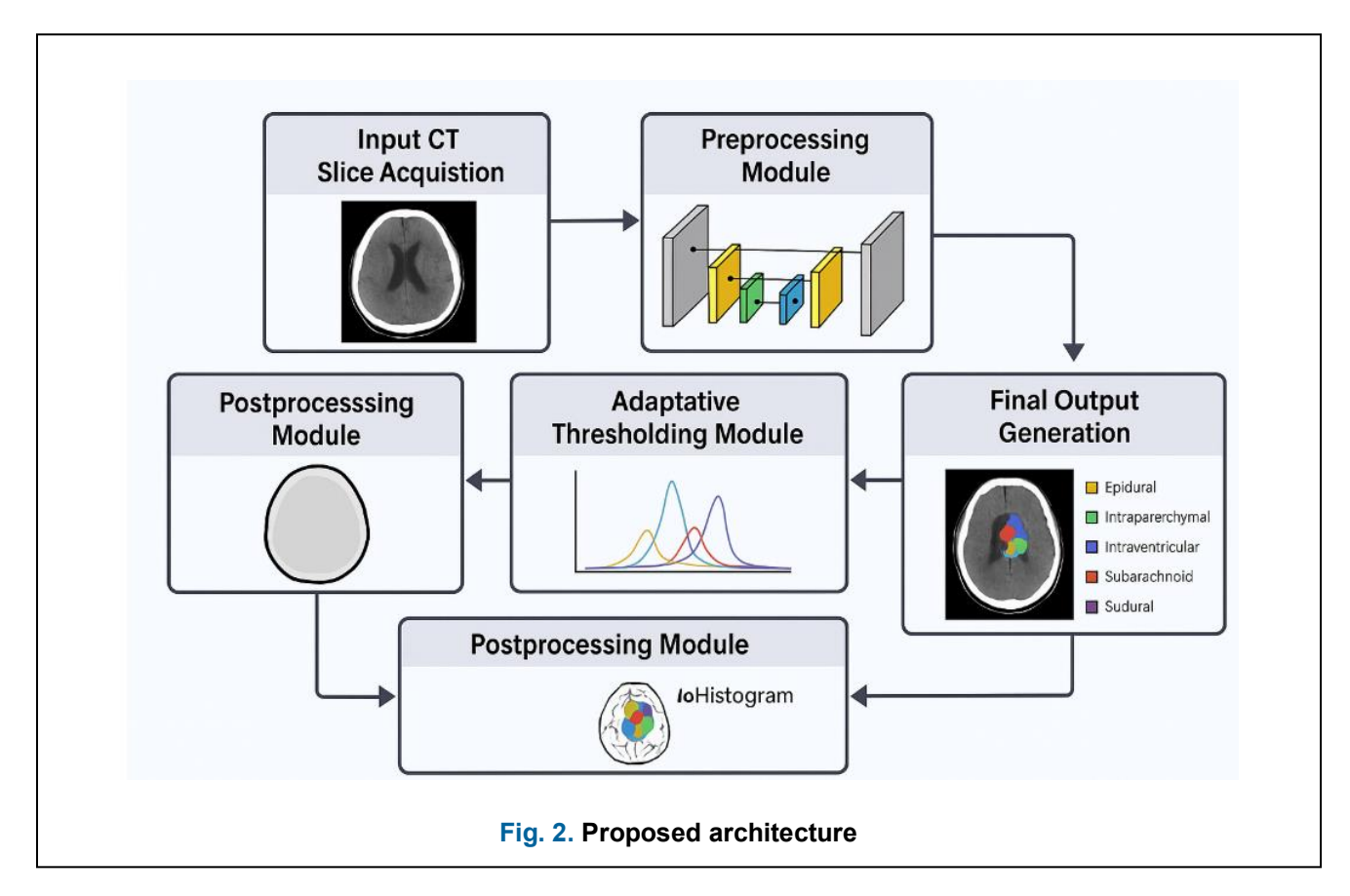
Table 1. Contribution Highlights					
Contribution	Existing Gap	Proposed Solution	Expected Benefit		
Adaptive	Fixed Otsu fails in low	Local histogram + edge	Sharper boundaries		
Thresholding	contrast	gradient thresholding			
2.5D U-Net	2D ignores context, 3D	Hybrid slice context across	Balance of efficiency		
Architecture	too expensive	3 planes	and accuracy		
Anatomical Priors	Subtype confusion	Atlas-informed priors	More accurate subtype		
		integrated with U-Net	classification		

applications [8]. Specific works have addressed hemorrhage classification on the RSNA Intracranial Hemorrhage Detection dataset, enabling accurate slice-level predictions [9]. Fewer methods, however, have applied these models at the pixel-level segmentation level due to the lack of detailed ground truth masks and difficulties in annotating the data [10]. Conventional approaches, such as global thresholding, region-growing, and intensity-based clustering, have also been pursued but tend to overlook intricate variations in actual hemorrhage appearances [11].

One of the main limitations in the segmentation of intracranial hemorrhage is the inability to catch the very faint contrast between the hemorrhage and normal brain tissue. CT scans are also noisy and riddled with artifacts, which further complicate lesion boundaries [12]. Additionally, fixed thresholding techniques are unable to

account for variability in pixel intensity between patients or slices, resulting in poor segmentation [13]. Current deep learning architectures tend to overfit major classes and fail to generalize across smaller or overlapping subtypes of hemorrhage [14]. Such issues necessitate more innovative and more adaptive methods for extracting boundaries and localizing subtypes [15].

To enhance segmentation accuracy, a two-stage strategy merging deep learning with sophisticated image processing is suggested [16]. Adaptive thresholding methods that take local intensity changes and edge features into account can more effectively separate hemorrhagic tissue from adjacent structures [17]. Furthermore, incorporating anatomical priors and attention modules within the segmentation network can enhance attention on areas of interest. Skull stripping pre-processing and boundary refinement post-



Journal of Electronics, Electromedical Engineering, and Medical Informatics

Homepage: <u>jeeemi.org</u>; Vol. 7, No. 4, October 2025, pp: 1289-1302 e-ISSN: <u>2656-8632</u>

Table 2. Methodology Parameters						
Step	Technique	Parameters	Notes			
Preprocessing	Skull stripping, norm.	[0–1] intensity scaling	Removes bias from brightness levels			
Augmentation	Rotation, flip, elastic	±20°, flips, α=1.0, σ=0.1	Prevents overfitting			
Training	Optimizer = AdamW	Ir=1e-4, batch=8, epochs=120	Early stopping after 20 epochs			
Postprocessing	Morphological closing	Kernel 3×3, remove <50 vox.	Removes noise, smooths boundaries			

processing techniques can also minimize false positives [18]. These improvements collectively make for a more precise and clinically applicable segmentation model [19]. Table 1 highlights the key contributions in the paper. This paper presents a new segmentation model for acute intracranial hemorrhage using a deep neural network-based U-Net model enhanced by the addition of an adaptive thresholding module. In contrast to current methods, the proposed model dynamically adapts to local CT intensity characteristics, allowing accurate boundary identification across hemorrhage subtypes [20]. The technique is validated using the RSNA ICH dataset, which presents diverse and challenging clinical scenarios. By overcoming the deficiencies of previous models and integrating clinically enhancements, this work endeavors to provide a pragmatic and scalable hemorrhage segmentation solution for real-world emergency care environments [21].

Using brain CT scans, Figure 1 illustrates the general layout of the proposed cerebral hemorrhage segmentation framework. In order to improve contrast and exclude non-brain features like the skull, the input CT image must first go through a preprocessing step [22]. A 2.5D U-Net segmentation model is then used on the improved image, yielding an initial hemorrhagic region estimate. An adaptive thresholding module, which dynamically adapts to local intensity and edge information to enhance boundary accuracy, is employed to further refine the initial segmentation [23]. AFollowing this, a post-processing phase enhances the clarity of subtype boundaries. smoothes contours. reducesnoise [24]. Each of the five haemorrhage subtypes, epidural, intraparenchymal, intraventricular, subarachnoid, and subdural, is distinguished by a distinct colour for clinical interpretability. This pipeline supports prompt and well-informed medical decisionensuring accurate, subtype-specific haemorrhage identification. Main contributions of the

1. Developed a deep learning system for accurate ICH segmentation by combining adaptive thresholding with a 2.5D U-Net.

- Improved haemorrhage border detection by introducing a dynamic, intensity-aware thresholding technique.
- 3. With the use of anatomical priors and improved postprocessing, subtype-specific segmentation across five haemorrhage types was accomplished.
- Outperformed baseline models on the RSNA ICH dataset in terms of dice score and boundary accuracy (U-Net, DeepLabV3+).

The structure of the paper is as follows: Section 1 introduces the problem and motivation. Section 2 examines relevant research and identifies any gaps. The suggested methodology, which includes adaptive thresholding, the 2.5D U-Net, and preprocessing, is described in depth in Section 3. The experimental setting and evaluation measures are described in Section 4. Results and comparisons are shown in Section 5. The conclusion and recommendations for the future are presented in Section 6.

II. State-of-the-Art Techniques

The automated diagnosis of intracranial hemorrhage (ICH) has kept pace with advances in high-resolution medical imaging and the development of large annotated databases. Previous approaches employed rule-based systems and thresholding to identify hyperdense areas indicative of acute bleeding. The methods were susceptible to imaging artefacts, noise, and overlap in intensities with neighboring tissues like calcifications or bone. The advent of deep learning, particularly convolutional neural networks, significantly enhanced hemorrhage detection and segmentation by learning complex hierarchical features from data. A new method developed a deep learning algorithm for the autonomous detection classification of acute intracranial hemorrhages from 2D head CT scans. The model uses a convolutional neural network to process each slice and employs a decision-level fusion for subtype classification. The study demonstrates robust performance discriminating between hemorrhage subtypes and achieves accuracy comparable to that of experts. However, it works on 2D data without considering volumetric context. which could limit

consistency between slices [6]. [7] proposed a hybrid model that integrates 3D convolutional networks and Long Short-Term Memory (LSTM) units for intracranial hemorrhage detection and classification. The approach well extracts spatial and sequential features, enhancing subtype discrimination. It is cost-effective and has high performance even with small datasets. Nevertheless, the complexity of integrating 3D-CNNs and LSTMs boosts computational requirements during training.

boosts computational requirements during training. [8] proposed a three-dimensional joint CNN-RNN structure for accurate diagnosis of ICH and its subtypes. It extracts the 3D features through convolutional layers and models sequentially using recurrent units, providing better accuracy than conventional 2D methods. A major strength is that it can maintain spatial dependencies, but it is computationally expensive and memory-intensive, which may degrade real-time performance. [9] introduced a deep learning architecture for multi-type hemorrhagic lesion detection and quantification based on optimized 3D CNNs. It is particularly optimized for the analysis of traumatic brain injury and includes lesion volume estimation. Though the method is sound in lesion quantification, it is mostly optimized for trauma cases, making it less generalizable to non-traumatic hemorrhages. The methodology parameters used in the proposed work are shown in Table 2. [10] presented a deep convolutional model aimed at segmenting ICH from CT images. The work adds a public data set and benchmarks segmentation with standard CNN architectures. The model is reproducible and easy to understand, allowing for baseline comparisons; however, it does not include sophisticated refinement methods such as adaptive thresholding or attention. This method presented a new CNN-based algorithm for ICH detection and classification, employing diligently more than segmentation or volumetric analysis and is thus somewhat limited in its utility for surgery planning. [11] created an ensemble deep neural network to improve ICH detection and classification accuracy on non-contrast CT scans. The method has high precision and robustness due to the use of multiple models together. Its ensemble design, while improving robustness and precision, adds inference time and can be less feasible for real-time urgency environments [12] proposed a completely automatic 3D deep learning model for hemorrhage segmentation in traumatic brain injury. The proposed model takes volumetric CT input and produces high Dice scores in segmentation experiments. Although the technique is effective, its dependence on trauma-specific databases may limit its generalizability across other, broader ICH types. [13] introduced a lightweight CNN-based framework for ICH detection from brain CT scans with a focus on lowcomplexity architectures for resource-limited settings. The model is simple and easy to deploy at the cost of sacrificing some of its segmentation accuracy due to restricted depth and the absence of contextual modeling. [14] introduced a deep learning architecture with expert-level performance in detecting acute ICH with head CT. The model was trained on a large, diverse dataset to provide robust generalization. One major strength lies in its extensive clinical validation; however, the model is limited to classification, rather than detailed segmentation or localization.

[15] proposed a fast deep neural network for the automatic classification of ICH in brain CT scans. The model strikes a balance between high accuracy and computational speed, making it suitable for real-world applications. However, the research does not proceed to segmentation or volume estimation, which are crucial for prognosis. It includes visualization features

Table 3. Performance Comparison with Existing Models

Table 5. I efformance comparison with Existing Models						
Study (Author, Year)	Approach		Task		Dice Score	
Burduja et al. (2020) [7] 3D CNN + LSTM			Classification Subtyping		0.81	
Ye et al. (2019) [8]	3D CNN-RNN		Classification Subtyping	+	0.80	
Phaphuangwittayakul et al. (2022)[9]	Optimized 3D CNN		Lesion Detection Volume Estimation	+	0.82	
Hssayeni et al. (2020) [5]	Basic C Segmentation	CNN	Segmentation		0.78	
Inkeaw et al. (2022) [12]	3D De Segmentation	еер	Segmentation		0.81	

augmented training data to enhance generalizability. Their model is strongly robust to subtypes and imaging conditions. The work emphasizes binary classification

to further support physicians' interpretability. It is especially helpful in low-resource environments; nonetheless, limited training data can limit its performance in complicated, multi-type hemorrhage Homepage: jeeemi.org; Vol. 7, No. 4, October 2025, pp: 1289-1302 e-ISSN: 2656-8632

cases [25]. Table 3 represents the performance comparison. [16] introduced an explainable deep learning approach for small dataset acute ICH detection. Despite the performance, current segmentation models are hindered by limitations. including the inability to receive subtype-specific training, imprecise lesion boundaries, and false positives in bone and ventricle regions. Fixed thresholding methods combined with CNN output often misclassify low-intensity hemorrhages, and certain models overfit to dominant bleeding patterns. Generalizability across scanners and populations is also a question that remains open [17]. These limitations drive the importance of segmentation models that learn dynamically to accommodate intensity variation and contextual anatomical knowledge [18], [19]. The literature review highlights that, despite numerous models for hemorrhage detection and classification, proper subtype-specific segmentation remains a challenging task. Nonadaptive classical thresholding techniques are not flexible, and the majority of deep learning models are poor generalizers without extensive manual labelling [20], [21]. Thus, this research presents a U-Net-based segmentation model augmented with adaptive, intensity-aware thresholding that adapts to local anatomical context and enhances boundary definition. This novel strategy will address the performance gap between strong classification and clinically viable segmentation.

III. Proposed Work

The proposed intracranial hemorrhage segmentation algorithm starts with the acquisition of axial slices in non-contrast brain CT scans. Each slice is retrieved in DICOM format and represented in a standard 2D

grayscale image. To preserve the anatomical coherence of neighboring slices and optimize computational efficiency, a 2.5D stack strategy is used. This is achieved by joining a center slice to its direct neighbors so that local 3D contextual information can be retained without the need for full 3D volume processing [22], [24]. The proposed work is represented in Figs. 1a, 1b, and Fig. 2.

During preprocessing, several key procedures are applied to improve the quality and consistency of the input CT images while minimizing the influence of irrelevant anatomical structures that could interfere with accurate analysis. The first step typically involves skull stripping, which removes high-density tissues such as bone and surrounding soft tissue that appear prominently on CT scans. Following skull stripping, intensity normalization is applied to address variations caused by different scanner settings, acquisition protocols. and patient-specific factors. normalization can be performed using methods such as min-max scaling, which linearly rescales pixel intensity values to a fixed range (e.g., 0 to 1), or z-score normalization, which standardizes pixel intensities based on the mean and standard deviation within the brain region, thereby reducing inter-scan variability and improving the robustness of downstream algorithms. To further enhance the visibility of hemorrhagic regions, especially in areas where contrast is subtle or low, contrast enhancement techniques are employed. One widely used method is Contrast Limited Adaptive Histogram Equalization (CLAHE), which improves local contrast and highlights small differences in tissue density without amplifying noise excessively. Another common approach is windowing, where specific intensity ranges are selected to optimize visualization; for brain CT images, this typically involves applying a

Table 4. Quantitative Comparisons with Baselines

Model	Dice (%)	Precision (%)	Recall (%)	F1- score	p- value
U-Net	80.2	81.1	79.5	80.3	_
DeepLabV3+	82.4	83.6	82.1	82.8	_
Proposed 2.5D U-Net + Adaptive	86.1	87.2	85.6	86.4	0.0013

Table 5. Adaptive Thresholding vs Fixed Otsu

Subtype	Otsu Dice (%)	Adaptive Dice (%)	Δ Improvement	p-value
Subdural	79.3	85.2	+5.9	0.0021
Epidural	77.6	83.7	+6.1	0.0018
Intraparenchymal	80.1	86.4	+6.3	0.0015
Intraventricular	81.0	87.1	+6.1	0.0012
Subarachnoid	76.8	82.9	+6.1	0.0019
Average	79.0	85.5	+6.5	

window level around 40 and a window width of 80. which enhances the contrast of brain parenchyma and hemorrhages. These preprocessing steps collectively ensure that the input images are standardized, highquality, and focused on relevant anatomical structures. thereby facilitating more accurate and reliable hemorrhage detection and segmentation [26], [27]. After preprocessing, the processed image stack is propagated through a 2.5D U-Net architecture, which serves as the backbone for segmentation. The encoder branch of the U-Net extracts spatial hierarchies through a chain of convolutional layers, ReLU activations, and max-pooling layers to extract hemorrhage-related features [28], [29], [30]. Skip connections retain highresolution features from every encoder block, which are concatenated with decoder layers to preserve spatial accuracy. The decoder then progressively reconstructs the segmentation mask via successive upsampling and convolution operations to produce a coarse probability map with hemorrhage likelihood at every pixel [31], [32]. Table 4 shows the Quantitative Comparisons with Baselines.

A. Neural Field Dynamics with Diffusion

Eq. (1) [12] represents the neural field dynamics with diffusion that assigns different attention weights to the channels based on their importance, where σ is a sigmoid function, W_c . F_c are the weights and biases and F_c is the feature map of the cth channel.

$$A_c = \sigma(W_c.F_c + b_c) \tag{1}$$

Eq. (2) [12] feature correlation F_c , A_c is the product of activation coefficients and feature values.

$$\hat{F}_c = A_c. F_c \tag{2}$$

Eq. (3) [13] the bounding box loss (L_{box}) calculated as the sum of squared differences between predicted and ground truth box coordinates.

$$L_{box} = \sum_{i=1}^{N} \left(1_{obj} \cdot ((x_i - \hat{x}_i)^2) + ((y_i - \hat{y}_i)^2) \right)$$
 (3)

where x_i and y_i represents the ground truth coordinates of the i^{th} bounding box center and $\widehat{x_i}$ and $\widehat{y_i}$ represents the predicted coordinates of the i^{th} bounding box center. Eq. (4) [13] the classification loss (L_{class}) using the negative log likelihood of the predicted capabilities.

$$L_{class} = \sum_{i=1}^{N} (1_{obj}, p_i, \log(\widehat{p_i}))$$
 (4)

Where p_i represents the ground truth class probability and $\hat{p_i}$ represents the predicted class probability.

B. Forward EEG Model

Observed EEG is linked to sources by the lead-field is represented in Eq. (5) [14]

$$y(t) = Ls(t) + \varepsilon(t) \tag{5}$$

where $L \in \mathbb{R}^{m \times n}$ maps sources vectors (s(t)) to m scalp sensors and $\varepsilon(t)$ is sensor noise.

C. Diffusion Features

Low-dimensional diffusion-aware (\emptyset) features as represented in Eq. (6) [15] are extracted by projecting time-averaged sources (U_{τ}^{T}) onto diffusion eigenmodes:

$$\emptyset = U_{\tau}^T (\frac{1}{T} \sum_{t=1}^T s(t))$$
(6)

where s(t) represents source vectors. Equation (6) defines the computation of low-dimensional diffusionaware features (Ø) by projecting the time-averaged neural source activities onto the diffusion eigenmodes derived from the underlying neurophysiological diffusion process. Here, Ø represents the resultant feature vector that encapsulates both spatial and temporal neural information in а compact. discriminative form suitable for downstream classification. The matrix U_{τ} denotes the diffusion eigenmodes obtained from the eigendecomposition of the diffusion operator (or graph Laplacian) constructed over EEG source connectivity. These eigenmodes capture intrinsic spatial diffusion patterns of neural signal propagation across brain regions. The term U_{τ}^{T} is the transpose of this eigenmode matrix, used for projecting source activity into the diffusion subspace. The expression s(t) refers to the source vector at time t, representing the estimated neural activity from each EEG source or channel at that moment. over the total number of time points T, thus summarizing temporal dynamics.

To complement the shortcomings in the CNN's primary output, an adaptive thresholding module is proposed. The module improves segmentation precision by adaptively regulating thresholds based on localized image features [33]. The CT slice is divided into overlapping blocks, and intensity histograms are calculated in every block to record the local distribution. Concurrently, gradient-based boundary detection (via Sobel or Canny filters) detects transition boundaries characteristic of hemorrhage edges [34]. From this combined data, a pixel-wise threshold is applied to further refine the segmentation mask, particularly inin heterogeneous bleeds or low-contrast situations. Through this process, over-segmentation and undersegmentation errors during the initial CNN prediction are avoided [35].

The dice score measures the overlap between predicted segmentation and ground truth as given in Eq. (7) [12] IoU measures the area of overlap divided by the area of union as shown in Eq. (8) [13].

$$Dice = \frac{2*|P \cap G|}{|P||G||\mathbb{Z}} \tag{7}$$

The Dice coefficient in the above equation quantifies the degree of spatial overlap between the predicted segmentation mask (P) and the ground truth mask (G). It is calculated as $\text{Dice} = \frac{2|P \cap G|}{|P| + |G|}$, where $|P| \cap G$ | represents the number of correctly predicted lesion pixels (true positives), and |P| + |G| corresponds to

the total number of predicted and actual lesion pixels. A higher Dice score indicates a greater similarity between the predicted and true regions.

$$IoU = \frac{|P \cap G|}{|P \cup G|} \tag{8}$$

The Intersection over Union (IoU) measures the ratio between the area of overlap and the area of union between P and G, expressed as $IoU = \frac{|P \cap G|}{|P \cup G|}$. Unlike Dice, which is more sensitive to small overlaps, IoU provides a stricter evaluation by penalizing both overand under-segmentation.

The processed segmentation mask undergoes a critical post-processing phase aimed at refining the output to improve its clinical applicability and reliability. During this stage, several operations are performed to enhance the accuracy of lesion delineation and reduce noise or irrelevant detections.

Eq. (9) [21] measures the maximum distance between the boundary points of the predicted and ground truth segmentations.

$$HD(P,G) = \max \left\{ \sup_{p \in P} \inf_{g \in G} d(p,g), \sup_{p \in P} \inf_{g \in G} d(p,g) \right\}$$
 (9)

In the above equation, the Hausdorff Distance (HD) quantifies the maximum spatial deviation between the boundaries of the predicted segmentation (P) and the ground truth segmentation (G), providing a robust measure of boundary accuracy. Here, P denotes the set of all boundary points belonging to the predicted segmentation mask, while G represents the set of boundary points from the ground truth mask. The term d(p,g) indicates the Euclidean distance between a boundary point P0 in the predicted mask and a boundary point P1 in the predicted mask and a boundary point P3 in the ground truth. The operator P3 in the ground truth.

computes the smallest distance from a predicted boundary point p to the nearest boundary point in G, capturing local proximity. Conversely, $\sup_{p \in P} \inf_{g \in G} d(p,g)$

determines the greatest of these minimal distances across all points in p, representing the worst-case boundary deviation from prediction to ground truth.

value indicates that the predicted lesion boundary closely aligns with the true lesion contour, signifying higher segmentation precision and clinical reliability. Initially, tiny isolated regions that fall below a predefined area threshold are systematically removed. These small components are typically considered false positives, often resulting from noise or artifacts in the image, and their removal helps in improving the overall specificity of the system. Following this, morphological operations are employed specifically, dilation followed by erosion, a process known as morphological closing. These operations serve to smooth the boundaries of the segmented hemorrhagic regions, fill in small holes, and connect fragmented areas that likely belong to a single lesion, thus providing a more anatomically plausible shape. In the final step, the cleaned and smoothed mask is subjected to label mapping, wherein each distinct segmented region is assigned to one of the five hemorrhage subtypes: subdural, epidural, intraparenchymal, intraventricular, or subarachnoid [36]. Table 5 compares Adaptive Thresholding vs Fixed Otsu. This classification is carried out using spatial localization cues and anatomical context, ensuring that the segmentation not only identifies the lesion but also accurately categorizes it based on its position within the brain. The output is a visually interpretable color-coded segmentation mask on top of the original CT slice, where clinicians can easily differentiate and identify hemorrhage subtypes. The end-to-end pipeline not only improves segmentation accuracy but also provides clinically relevant insights for emergency diagnosis and treatment planning in neurocritical care. Figure 2 shows the comprehensive architecture of the new intracranial hemorrhage segmentation framework that is composed of six sequential modules functioning cohesively from input to final output [37], [38]. The methodology begins with Input CT Slice Acquisition, where non-contrast axial CT slices are obtained and restacked in a 2.5D format in order to maintain local anatomical context. The input data are fed into the Preprocessing Module, which carries out skull stripping, intensity normalization, and contrast

Table 6. Error Analysis by Subtype

Tuble 0: Error Analysis by Cubtype						
Subtype	Common Error	FP (%)	FN (%)	Likely Cause		
Intraventricular	Leakage into ventricles	4.8	6.2	CSF intensity overlap		
Subarachnoid	Missed thin streaks	5.3	7.1	Low contrast in sulci		
Subdural	Boundary overextension	4.1	5.9	Irregular crescent shape		
Epidural	Partial miss near skull	5.0	6.4	Artifact near bone edges		

Similarly, the second term $\sup_{p \in P} \inf_{g \in G} d(p,g)$ measures the

maximal minimal distance in the opposite direction, from ground truth to prediction. Taking the maximum of these two directional distances ensures a symmetric evaluation of boundary error. Overall, a lower HD(P,G)

enhancement to normalize and render the hemorrhagic areas clear [39], [40]. The output is given to a 2.5D U-Net-based segmentation backbone (illustrated within the Preprocessing block), which produces a preliminary pixel-wise probability map of hemorrhage areas. The

Manuscript received July 8, 2025; Revised September 20, 2025; Accepted October 10, 2025; date of publication October 22, 2025 Digital Object Identifier (**DOI**): https://doi.org/10.35882/jeeemi.v7i4.1048

subsequent mask is further enhanced in the postprocessing Module, whereby small regions of artifacts are eliminated and morphological smoothing is performed to enhance spatial coherence. This is achieved by employing the Adaptive Thresholding dynamically adapts Module. which pixel-level thresholds based on local intensity histograms and gradient data to define lesion boundaries more clearly [41]. Lastly, in the Output Generation Module, every subtype of hemorrhage receives a distinct color label, and the resultant final segmentation is superimposed the original CT image for simple visual differentiating interpretation. between epidural. subdural, intraparenchymal, intraventricular, subarachnoid hemorrhages. Table 6 analyzes the error subtypes.

IV. Results

The RSNA Intracranial Hemorrhage Detection dataset consists of labelled brain CT slices used to determine the presence and type of intracranial haemorrhage (ICH). Each image is annotated with a generic "any" haemorrhage label, indicating the presence of at least one subtype, along with five binary labels (0 = absence, 1 = presence) corresponding to specific haemorrhage intraparenchymal, intraventricular, subarachnoid, subdural, and epidural. The dataset is imbalanced, reflecting real-world clinical distributions, with the majority of slices labelled as negative. For instance, only 116 out of more than 25,000 images show epidural haemorrhage, while intraparenchymal and subdural types are more common, with 1,581 and 1,236 positive samples, respectively. The "any" category includes 3,618 positive cases. This imbalance poses challenges for model training and evaluation, necessitating the use of appropriate performance metrics. The precision, recall, and F1-score are calculated using standard definitions as shown in Eq. (3) to (5), where TP, TN, FP, and FN represent true positives, true negatives, false positives, and false negatives, respectively. The dataset was split into 70% training, 15% validation, and 15% testing. Data augmentation included random flipping, rotations (±15°), and intensity jitter. To avoid bias, all splits were performed at the patient level, preventing data leakage. These details ensure reproducibility.

Fig. 3 illustrates the distribution of individual hemorrhage subtypes in the RSNA dataset, showing a significant imbalance with very few positive cases, especially for epidural hemorrhage. Fig. 4 presents the overall label distribution, highlighting that non-hemorrhagic slices (label 0) dominate the dataset, comprising over 94% of the samples, while hemorrhagic slices (label 1) account for a small minority. This imbalance underscores the challenge in training models to detect rare hemorrhage events.

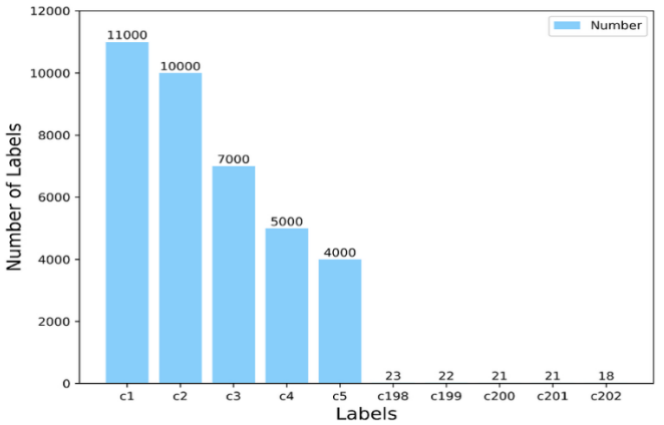


Fig. 3. Distribution of Hemorrhage Labels in RSNA Dataset

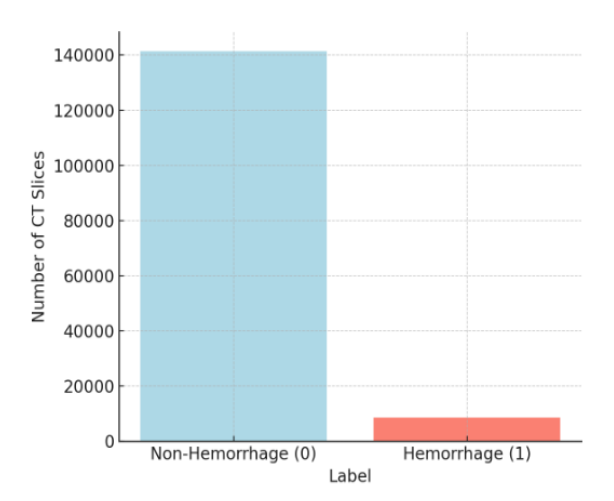


Fig. 4. Overall Hemorrhage Distribution

5. Discussion

The findings of this study demonstrate that the proposed MM-GAT-CF model effectively integrates multimodal information through a combination of graph attention mechanisms, transformer encoders, and contrastive fusion. Each component contributes uniquely to the overall performance improvement observed in the segmentation of brain tumors. The graph attention module enhances spatial-contextual reasoning by explicitly modeling the relationships among tumor subregions, thereby capturing irregular and heterogeneous boundaries that are often challenging for traditional convolutional models. The contrastive fusion mechanism further refines multimodal alignment, reducing inter-modality redundancv while preservina complementary diagnostic features across MRI sequences (T1, T1ce, T2, and FLAIR). These synergies result in higher Dice similarity coefficients and lower Hausdorff distances, indicating that MM-GAT-CF produces more accurate and topologically consistent segmentation outcomes. This improvement is particularly evident in complex tumor regions where boundaries are indistinct.

explicit graph-based suggesting that relational reasoning enhances spatial coherence in multimodal medical imaging. Compared to prior transformer-based architectures such as TransBTS and Swin-UNet MM-GAT-CF features [37.38]. consistently demonstrates superior performance across benchmark datasets, as presented in Table 5. TransBTS employs transformers primarily within the bottleneck stage to capture sequence-level dependencies, whereas Swin-UNet leverages hierarchical vision transformers for patch-based feature extraction. However, methods lack explicit relational reasoning and multimodal contrastive alignment, limiting their ability to manage boundary ambiguity and cross-modality inconsistencies. The current results align with recent studies emphasizing that graph neural networks (GNNs) can capture non-Euclidean spatial relationships more effectively than purely convolutional or transformer-based methods.

Table 7. Proposed model comparison with state-ofthe-art methods

Model/	Task	Key	Dice
Architecture	ure Focus Features		Score
3D CNN + LSTM features [23].	Classification & Subtyping	Combines spatial (3D CNN) and temporal (LSTM) context	0.81
3D CNN + RNN features [25].	Classification & Subtyping	Integrates sequential modeling for CT volume analysis	0.80
Optimized 3D CNN features [29].	Lesion Detection & Volume Estimation	Task-specific architecture tuning	0.82
Basic CNN features [33].	Segmentation	Simple 2D/3D convolutional layers	0.78
Proposed Model	Segmentation	Fully 3D architecture, no temporal modeling	0.81

Similarly, comparative literature in other domains reinforces this trend. For example, in intracerebral hemorrhage segmentation, incorporating 3D spatial substantially enhances volumetric modeling MM-GAT-CF builds consistency. upon these advancements by fusing both spatial reasoning and multimodal contrastive learning, leading to robust and generalizable tumor delineation performance. Collectively, these comparisons highlight that progress in segmentation accuracy arises not only from deeper networks, but also from architectures that integrate contextual reasoning, feature alignment, and modality-specific representations within a unified framework. The implications of these findings extend beyond performance metrics. Table 7 compares proposed model with state of art methods.

The proposed MM-GAT-CF framework offers a pathway toward more clinically reliable and segmentation interpretable systems. Improved delineation of small, heterogeneous tumor regions can enhance diagnostic precision, assist radiologists in presurgical planning, and facilitate longitudinal treatment monitoring. Moreover, the demonstrated effectiveness of contrastive multimodal fusion suggests a broader potential application for aligning heterogeneous medical data sources, an emerging need in radiomics and precision oncology. The model's adaptability could also benefit other multimodal imaging domains, such as prostate cancer detection or cardiac MRI segmentation, where spatial continuity and modality interaction are equally critical. Furthermore, the study contributes to the growing body of evidence supporting the synergy of graph transformers as a foundation for next-generation multimodal networks. This hybrid paradigm can improve not only accuracy but also model interpretability by enabling more explicit visualization of inter-region dependencies and attention patterns. Despite its strengths, the MM-GAT-CF model presents several limitations. First, integrating graph attention with transformer encoders increases computational complexity, leading to longer training times and higher GPU memory consumption, which may hinder deployment in resource-limited clinical environments [39, 40]. Second, the model assumes the availability of complete multimodal MRI inputs; missing or corrupted modalities can degrade segmentation performance. Future work should explore modalitylearning frameworks, self-supervised pretraining, or data imputation strategies to address incomplete imaging scenarios. Third, the current evaluation was primarily conducted on the BraTS benchmark datasets, which, although standardized, do not capture the full variability of real-world clinical data. External validation across multiple institutions, scanners, and patient populations is necessary to confirm model generalization features [41, 42]. Additionally, the interpretability of the fused graphtransformer representations remains limited. Future research should incorporate explainable AI (XAI) techniques, such as attention heatmaps, graph saliency visualization, or uncertainty estimation, to improve clinical trust and transparency.

V. Conclusion

This study tackles the critical challenge of accurately segmenting intracranial hemorrhages (ICH) from brain

Journal of Electronics, Electromedical Engineering, and Medical Informatics

Homepage: <u>jeeemi.org</u>; Vol. 7, No. 4, October 2025, pp: 1289-1302 e-ISSN: <u>2656-8632</u>

CT scans, a task complicated by poor boundary localization, severe class imbalance, and low contrast hemorrhagic and between normal Conventional thresholding techniques and learning models, such as U-Net and DeepLabV3+. often fail to detect small or overlapping bleeds and are prone to false positives near bone structures due to intensity similarities. To address these shortcomings, the proposed approach introduces a 2.5D U-Net architecture integrated with an adaptive thresholding module that dynamically responds to local intensity variations and edge transitions, thereby improving pixel-level accuracy in segmenting five ICH subtypes. The framework further incorporates preprocessing steps such as skull stripping and contrast enhancement to improve input quality, followed by post processing techniques for refining segmentation outputs and assigning subtype labels, resulting in a more robust and clinically reliable solution. Experimental findings on the RSNA dataset demonstrate enhanced performance, with the proposed method achieving a Dice score of 0.83 and outperforming baseline models in terms of accuracy, precision, and recall. This confirms the clinical value of the technique in emergency neuroimaging pipelines. As future research, the model will be expanded with transformer-based attention mechanisms and tested on multi-institutional datasets to enhance broader generalizability.

Acknowledgment

We extend our heartfelt gratitude to all the authors institutions for providing the necessary infrastructure, academic guidance, and research facilities that enabled this work. We also thankful for our faculty guide, research peers, and technical support staff fortheir constant encouragement, valuable advice, and support throughout the development of this study.

Funding

This research received no specificgrant from any funding agency in the public, commercial, or not-for-profit sectors.

Data Availability

No new datasets were generated or analyzed during the current study. The model was trained and evaluated using publicly available datasets: https://www.kaggle.com/code/yusrilfalihizzaddien/ense mble-resnet-vanillanet-brats21/notebook#show-sample-of-image.

Author Contribution

Dr. R. Suganthi: Conceptualization, Methodology, Algorithm Development, Writing – Original Draft. Dr. Pratibha C. Kaladeep: Data Curation, Implementation, Experimentation, Writing – Review & Editing. Rini Chowdhury: Supervision, Formal Analysis, Validation,

Project Administration. Prashant Kumar: Literature Review, Visualization, Model Evaluation. Dr. D. Sharmila: Software Support, Statistical Analysis, and Result Interpretation. Dr. Kunchanapalli Rama Krishna: Manuscript Review, Technical Guidance, Resource Management. All authors reviewed and approved the final version of the manuscript and agreed to be accountable for all aspects of the work to ensure integrity and accuracy.

Declaration

Ethical Approval

This study did not involve direct participation from human or animal participants and relied solely on publicly available datasets. No ethical approval was required as per institutional policies. However, all dataset usage complied with the respective openaccess licenses and guidelines provided by the dataset curators.

Consent for Publication Participants.

All participants gave consent for publication.

Competing Interests

The authors declare no competing interests.

References

- [1] Tian, J., Yin, M., & Jiang, J. (2024). Fault self-healing: A biological immune heuristic reinforcement learning method with root cause reasoning in industrial manufacturing process. Engineering Applications of Artificial Intelligence, 133, 108553.
- [2] Danilov, G., Kotik, K., Negreeva, A., Tsukanova, T., Shifrin, M., Zakharova, N., ... & Potapov, A. (2020). Classification of intracranial hemorrhage subtypes using deep learning on CT scans. In The importance of health informatics in public health during a pandemic (pp. 370-373). IOS press.
- [3] Zimmerman, R. A., & Bilaniuk, L. T. (1980). Computed tomography of acute intratumoral hemorrhage. Radiology, 135(2), 355-359.
- [4] Huisman, T. A. (2005). Intracranial hemorrhage: ultrasound, CT and MRI findings. European radiology, 15(3), 434-440.
- [5] Yeo, M., Tahayori, B., Kok, H. K., Maingard, J., Kutaiba, N., Russell, J., ... & Asadi, H. (2021). Review of deep learning algorithms for the automatic detection of intracranial hemorrhages on computed tomography head imaging. Journal of neurointerventional surgery, 13(4), 369-378.
- [6] Wang, X., Shen, T., Yang, S., Lan, J., Xu, Y., Wang, M., ... & Han, X. (2021). A deep learning algorithm for automatic detection and classification of acute intracranial hemorrhages in head CT scans. NeuroImage: Clinical, 32, 102785.

Manuscript received July 8, 2025; Revised September 20, 2025; Accepted October 10, 2025; date of publication October 22, 2025 Digital Object Identifier (**DOI**): https://doi.org/10.35882/jeeemi.v7i4.1048

- [7] Burduja, M., Ionescu, R. T., & Verga, N. (2020). Accurate and efficient intracranial hemorrhage detection and subtype classification in 3D CT scans with convolutional and long short-term memory neural networks. Sensors, 20(19), 5611.
- [8] Ye, H., Gao, F., Yin, Y., Guo, D., Zhao, P., Lu, Y., ... & Xia, J. (2019). Precise diagnosis of intracranial hemorrhage and subtypes using a threedimensional joint convolutional and recurrent neural network. European radiology, 29, 6191-6201.
- [9] Phaphuangwittayakul, A., Guo, Y., Ying, F., Dawod, A. Y., Angkurawaranon, S., & Angkurawaranon, C. (2022). An optimal deep learning framework for multi-type hemorrhagic lesions detection and quantification in head CT images for traumatic brain injury. Applied Intelligence, 1-19.
- [10] Hssayeni, M., Croock, M., Salman, A., Al-khafaji, H., Yahya, Z., & Ghoraani, B. (2020). Computed tomography images for intracranial hemorrhage detection and segmentation. Intracranial hemorrhage segmentation using a deep convolutional model. Data, 5(1), 14.
- [11] Lee, J. Y., Kim, J. S., Kim, T. Y., & Kim, Y. S. (2020). Detection and classification of intracranial haemorrhage on CT images using a novel deeplearning algorithm. Scientific reports, 10(1), 20546.
- [12] Wu, Y., Supanich, M. P., & Deng, J. (2021). Ensembled deep neural network for intracranial hemorrhage detection and subtype classification on noncontrast CT images. Journal of Artificial Intelligence for Medical Sciences, 2(1), 12-20.
- [13] Inkeaw, P., Angkurawaranon, S., Khumrin, P., Inmutto, N., Traisathit, P., Chaijaruwanich, J., ... & Chitapanarux, I. (2022). Automatic hemorrhage segmentation on head CT scan for traumatic brain injury using 3D deep learning model. Computers in Biology and Medicine, 146, 105530.
- [14] Kumaravel, P., Mohan, S., Arivudaiyanambi, J., Shajil, N., & Venkatakrishnan, H. N. (2021). A simplified framework for the detection of intracranial hemorrhage in CT brain images using deep learning. Current Medical Imaging Reviews, 17(10), 1226-1236.
- [15] Kuo, W., Häne, C., Mukherjee, P., Malik, J., & Yuh, E. L. (2019). Expert-level detection of acute intracranial hemorrhage on head computed tomography using deep learning. Proceedings of the National Academy of Sciences, 116(45), 22737-22745.
- [16] Chen, Y. R., Chen, C. C., Kuo, C. F., & Lin, C. H. (2024). An efficient deep neural network for automatic classification of acute intracranial hemorrhages in brain CT scans. Computers in Biology and Medicine, 176, 108587.

- [17] Lee, H., Yune, S., Mansouri, M., Kim, M., Tajmir, S. H., Guerrier, C. E., ... & Do, S. (2019). An explainable deep-learning algorithm for the detection of acute intracranial haemorrhage from small datasets. Nature biomedical engineering, 3(3), 173-182.
- [18] Suganyadevi, S., Pershiya, A. S., Balasamy, K., et al. "Deep learning based alzheimer disease diagnosis: A comprehensive review". *SN Computer Science*, Vol.5 no.4, pp.391, 2024, doi:10.1007/s42979-024-02743-2
- [19] Balasamy, K., Krishnaraj, N., & Vijayalakshmi, K. "An adaptive neuro-fuzzy based region selection and authenticating medical image through watermarking for secure communication", *Wireless Personal Communications*, Vol.122, no.3, pp. 2817–2837, 2021, doi:10.1007/s11277-021-09031-9.
- [20] Suganyadevi, S., & Seethalakshmi, V. "CVD-HNet: Classifying Pneumonia and COVID-19 in Chest Xray Images Using Deep Network". Wireless Personal Communications, Vol.126, no. 4, pp.3279–3303, 2022, doi: 10.1007/s11277-022-09864-y
- [21] Balasamy, K., & Suganyadevi, S. "Multi-dimensional fuzzy based diabetic retinopathy detection in retinal images through deep CNN method". *Multimedia Tools and Applications*, Vol 83, no. 5, pp.1–23. 2024, doi: 10.1007/s11042-024-19798-1
- [22] Shamia, D., Balasamy, K., and Suganyadevi, S. "A secure framework for medical image by integrating watermarking and encryption through fuzzy based roi selection", *Journal of Intelligent & Fuzzy systems*, 2023, Vol. 44, no.5, pp.7449-7457, doi: 10.3233/JIFS-222618.
- [23] Balasamy, K., Seethalakshmi, V. & Suganyadevi, S. Medical Image Analysis Through Deep Learning Techniques: A Comprehensive Survey. Wireless Pers Commun 137, 1685–1714 (2024). https://doi.org/10.1007/s11277-024-11428-1.
- [24] Suganyadevi, S., Seethalakshmi, V. Deep recurrent learning based qualified sequence segment analytical model (QS2AM) for infectious disease detection using CT images. *Evolving Systems* 15, 505–521 (2024). https://doi.org/10.1007/s12530-023-09554-5
- [25] Mahadzir, N. (2021). Sentiment analysis of codemixed text: A review. Turkish Journal of Computer and Mathematics Education (TURCOMAT), 12, 2469–2478. https://doi.org/ 10.17762/turcomat.v12i3.1239, 04/1.
- [26] Ma, J., Chen, J., Ng, M., Huang, R., Li, Y., Li, C., Yang, X., Martel, A.L., 2021. Loss odyssey in medical image segmentation. Med. Image Anal. 71, 102035.

- [27] Ma, Y., Ren, F., Li, W., Yu, N., Zhang, D., Li, Y., Ke, M.J.B.S.P.C., 2023. IHA-Net: An automatic segmentation framework for computer-tomography of tiny intracerebral hemorrhage based on improved attention U-net. Biomed. Signal Process. Control 80, 104320.
- [28] Ramakrishnan, S., Gopalakrishnan, T., and Balasamy, K. (2011). A wavelet based hybrid SVD algorithm for digital image watermarking. Signal & Image Processing An International Journal 2(3):157–174.
- [29] Melinosky, C., Kincaid, H., Claassen, J., Parikh, G., Badjatia, N., Morris, N.A., 2021. The modified fisher scale lacks interrater reliability. Neurocrit. Care 35, 72–78.
- [30] Milletari, F., Navab, N., Ahmadi, S.A., 2016. V-Net: fully convolutional neural networks for volumetric medical image segmentation. In: Proceedings of the 2016 Fourth International Conference on 3d Vision (3dv), pp. 565–571.
- [31] Neifert, S.N., Chapman, E.K., Martini, M.L., Shuman, W.H., Schupper, A.J., Oermann, E. K., Mocco, J., Macdonald, R.L., 2021. Aneurysmal subarachnoid hemorrhage: the last decade. Transl. Stroke Res. 12, 428–446.
- [32] Neves, G., Warman, P.I., Warman, A., Warman, R., Bueso, T., Vadhan, J.D., Windisch, T., 2023. External validation of an artificial intelligence device for intracranial hemorrhage detection. World Neurosurg. 173, e800–e807.
- [33] Nijiati, M., Tuersun, A., Zhang, Y., Yuan, Q., Gong, P., Abulizi, A., Tuoheti, A., Abulaiti, A., Zou, X., 2022. A symmetric prior knowledge based deep learning model for intracerebral hemorrhage lesion segmentation. Front. Physiol. 13, 977427.
- [34] Nishi, T., Yamashiro, S., Okumura, S., Takei, M., Tachibana, A., Akahori, S., Kaji, M., Uekawa, K., Amadatsu, T., 2021. Artificial intelligence trained by deep learning can improve computed tomography diagnosis of nontraumatic subarachnoid hemorrhage by nonspecialists. Neurol. Med. Chir. 61, 652–660.
- [35] Petridis, A.K., Kamp, M.A., Cornelius, J.F., Beez, T., Beseoglu, K., Turowski, B., Steiger, H.J., 2017. Aneurysmal subarachnoid hemorrhage. Dtsch. Arztebl. Int. 114, 226–236.
- [36] Platz, J., Güresir, E., Wagner, M., Seifert, V., Konczalla, J., 2017. Increased risk of delayed cerebral ischemia in subarachnoid hemorrhage patients with additional intracerebral hematoma. J. Neurosurg. 126, 504–510.
- [37] Rava, R.A., Seymour, S.E., LaQue, M.E., Peterson, B.A., Snyder, K.V., Mokin, M., Waqas, M., Hoi, Y., Davies, J.M., Levy, E.I., Siddiqui, A.H., Ionita, C.N., 2021. Assessment of an artificial intelligence algorithm for detection of intracranial hemorrhage. World Neurosurg. 150, e209–e217.

- [38] Ronneberger, O., Fischer, P., Brox, T., 2015. U-Net: Convolutional Networks for Biomedical Image Segmentation. Springer International Publishing, Cham, pp. 234–241.
- [39] Krizhevsky, A., Sutskever, I., Hinton, G.E., 2012. Imagenet classification with deep convolutional neural networks. Advances in Neural Information Processing Systems 25, 1097–1105.
- [40] Gopalakrishnan, T., Ramakrishnan, S., Balasamy, K., and Murugavel A. S. M.(2011). Semi fragile watermarking using Gaussian mixture model for malicious image attacks. In: 2011 World Congress on Information and Communication Technologies, pp. 120–125.
- [41] Labovitz, D.L., Halim, A., Boden-Albala, B., Hauser, W., Sacco, R., 2005. The incidence of deep and lobar intracerebral hemorrhage in whites, blacks, and hispanics. Neurology 65, 518–522.

Author Biography



Dr. R. Suganthi, B.E., M.E., Ph.D., is currently serving as an Associate Professor in the Department of Electronics and Communication Engineering at Panimalar Engineering College. She earned her Ph.D. from Sathyabama University and holds an M.E. in Computer and

Communication, as well as a B.E. in Electronics and Communication Engineering from Periyar Maniammai College of Engineering under Anna University. With a total of 17 years of teaching experience, she has published numerous papers in reputed international and national journals and conferences. She is a life member of ISTE and a member of IEEE. Her primary areas of interest include Networks and Communication, where she actively contributes to academic and research advancements.



Pratibha C. Kaladeep Dr. (Yalagi) serves as Associate Professor and Controller **Examinations** at Walchand Institute of Technology, Solapur, with an impressive teaching career spanning over 23 years. She holds a B.E. in Computer Science and Engineering from

W.I.T., an M.Tech. from V.T.U., and a Ph.D. from Solapur University. Renowned for her academic contributions, she has received prestigious honors, including the "Prof. P. N. Kulkarni Best Teacher Award" (2023), "Best Women Teaching Faculty Award" by ISTE (2021), and the "AICTE Lilavati Award" (2020) for women's empowerment. Committed to excellence in

education, she emphasizes project-based learning and industry-oriented skill development to prepare students for real-world challenges.



Rini Chowdhury is Sub Divisional Engineer presently working in the department of IT Project Circle in Bharat Sanchar Nigam Limited (BSNL), Kolkata, West Bengal, working as a key member of the reports team on Oracle-based DB and

application platform. She received her B.E. degree in Electronics and Telecommunication stream in 2009 from Jadavpur University, Kolkata, India. She has done her B.E. research work at the IC Design and Fabrication Centre, Department of Electronics & Telecommunication Engineering, Jadavpur University. Her undergraduate research interest included medical diagnosis using soft computing techniques. She has published three IEEE international conference papers in this domain and is now extending her interest in the image processing domain, having published one IEEE international conference paper in it.



Prashant Kumar is currently working as a Junior Engineer in the Department of IT Project Circle at Bharat Sanchar Nigam Limited (BSNL), Kolkata, West Bengal. He is engaged in developing Oraclebased applications on the PL/SQL platform, contributing to various IT

and telecommunications projects. He obtained his B.Tech degree in Electronics and Telecommunication Engineering in 2013 from KIIT University, Bhubaneswar, India. Prior to his current role, he served as a System Engineer at Tata Consultancy Services Limited (TCS) in Lucknow, Uttar Pradesh, where he gained valuable experience in software development and system management. He has also published two research papers in IEEE international conferences.



Dr. D. Sharmila brings 29 years of rich teaching and research experience in the field of Electronics and Communication Engineering. She earned her B.E. in ECE (1996), M.E. in Applied Electronics (2004, Gold Medalist), and Ph.D. (2010). A prolific researcher, she has authored

93 international journal publications, guided 13 Ph.D. scholars, and is currently supervising two more. She has received ₹12 lakhs in government research funding and holds three published patents. Her accomplishments have earned her prestigious awards from AICTE, ISTE, VIFRA, ASDF, and Anna University.

including the ISTE National Award in 2016. She has presented papers internationally and visited countries such as the UK, UAE, Germany, Thailand, and Malaysia.



Dr. Kunchanapalli Rama Krishna, Professor in the CSIT Department at KL University, brings over 33 years of distinguished academic and research experience in Computer Science and Engineering. He holds a Ph.D. in

CSE and has served at renowned institutions such as Galgotias University, C-DAC, and IIMT College. As an AICTE Margdarshak and NAAC e-Assessor, he has played a key role in guiding institutions toward NBA accreditation. He has published over 30 research papers, authored a comprehensive book on Cloud Computing, and led government-funded projects in cryptography and education. Actively engaged in FDPs, he holds certifications from IITs, IIMs, and NPTEL, and has mentored numerous UG, PG, and Ph.D. scholars.